Spectrochimica Acta Part A: Molecular and Biomolecular Spectroscopy 273 (2022) 120900

Contents lists available at ScienceDirect

Spectrochimica Acta Part A: Molecular and Biomolecular Spectroscopy

journal homepage: www.elsevier.com/locate/saa

Assessment of bone dose response using ATR-FTIR spectroscopy: A potential method for biodosimetry

Pedro Arthur Augusto de Castro [a], Derly Augusto Dias [a], Matheus del-Valle [a], Marcelo Noronha Veloso [a], Elizabeth Sebastiana Ribeiro Somessari [b], Denise Maria Zezell [a,*]

[a] Center for Lasers and Applications, Nuclear and Energy Research Institute, IPEN – CNEN, 05508-000, Brazil
[b] Center for Radiation Technology, Nuclear and Energy Research Institute, IPEN – CNEN, 05508-000, Brazil

HIGHLIGHTS

- FTIR spectroscopy with PLS-DA enable the differentiation of the multiple ionizing doses on bone.
- FTIR spectroscopy can detect differences not only between the control group and ionizing radiation dose on bone but can also discriminate between the high and low radiation doses.
- The spectral features of carbonate accumulation, carbonate to mineral and mineral to matrix play an important role for bone dose response.

GRAPHICAL ABSTRACT

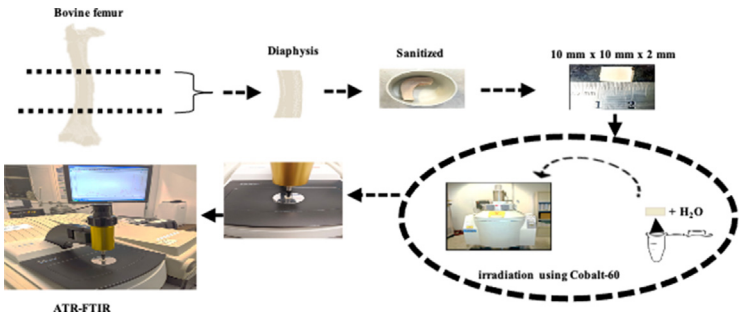

ARTICLE INFO

Article history:
Received 11 November 2021
Received in revised form 10 January 2022
Accepted 12 January 2022
Available online 16 January 2022

Keywords:
Ionizing Radiation
Biodosimetry
Chemometric
FTIR Spectroscopy
Bone
Gamma

ABSTRACT

The health care application of ionizing radiation has expanded worldwide during the last several decades. While the health impacts of ionizing radiation improved patient care, inaccurate handling of radiation technology is more prone to potential health risks. Therefore, the present study characterizes the bone dose response using bovine femurs from a slaughterhouse. The gamma irradiation was designed into low-doses (0.002, 0.004 and 0.007 kGy) and high-doses (1, 10, 15, 25, 35, 50 and 60 kGy), all samples received independent doses. The combination of FTIR spectroscopy and PLS-DA allows the detection of differences in the control group and the ionizing dose, as well as distinguishing between high and low radiation doses. In this way, our findings contribute to future studies of the dose response to track ionizing radiation effects on biological systems.

1. Introduction

The health care application of ionizing radiation has expanded worldwide during the last several decades [1]. It is estimated that more than 3,600 million diagnostic radiology examinations are performed annually, in which 7.5 million radiotherapy treatments are administered [2]. An established beneficial effect occurs on living organisms, such as improving the immune system [3], anti-inflammatory [4,5], radiation hormesis[6], cell growth stimulation [7], and lower mortality rate [8,9]. Additionally, radiation sterilization relies on ionizing radiation to deactivate microorganisms such as bacteria, fungi, viruses and spores [10,11]. It also could be a

* Corresponding author.
E-mail addresses: pedroarthur@usp.br (P. Arthur Augusto de Castro), matheus.valle@usp.br (M. Noronha Veloso), zezell@usp.br (D. Maria Zezell).

https://doi.org/10.1016/j.saa.2022.120900
1386-1425/

common method for the sterilization of connective tissue allografts, for example skin, cartilage, bone, tendons, heart valves and corneas [12]. Because of its effectiveness, ionizing radiation render as an essential technique for minimizing disease transmission and infection [12].

Advances in radiation technology have led to earlier diagnosis and less invasive treatments of human disease. However, even with the significant benefit of ionizing radiation in improving patient care, a thorough knowledge of the ionizing radiation consequences may reduce the overall health risk. Despite multiple studies investigating the health impacts of ionizing radiation, the effects of dose-rate and its possible implications are still not fully described [13]. Furthermore, recent developments in the field of biodosimetry have demonstrated that biological response to ionizing radiation depends not only on the radiation type and dose, but also on the type of biological system exposed and their response time [14]. Therefore, in the event of a large-scale radiological accident, sensitive and high-throughput diagnosis of victims is essential to evaluate the extent of radiation damage efficiently aiming to initiate medical treatment when necessary [15].

In the bone dose response context, the assessment of the molecular and cellular mechanisms of action induced by ionizing radiation can lead to the development of novel therapeutics capable of enhancing the efficacy of radiotherapy and adding support to irradiated autograft surgery [13]. Novel delivery methods are driven by an understanding of the fundamental physical interactions of radiation within biological tissue and the dependence of radiation damage response on those initial physical damages [15]. In this sense, Fourier transform infrared (FTIR) spectroscopy is an optical method that has been widely adopted in biomedical research as it provides high-speed background-free information regarding the vibrational modes of biological molecules, and thereby enables a correlation between spectral features and structural changes [16,17].

Biomolecules such as lipids, proteins, nucleic acids, and carbohydrates play an important role in the FTIR spectrum [18]. Their biochemical activities can be evaluated through alterations in peak positions, band shapes, intensities, and band area values [18,19]. Therefore, the aim of this study is to profile subtle changes in the biochemical content of bone dose response using FTIR spectroscopy combined with chemometric analysis.

2. Material and methods

2.1. Bone processing

The specimens of bovine femurs were purchased from a slaughterhouse that is certified to process bones and kept at −20 °C. Experimental procedures were conducted under the guidance of the institutional Ethics Committee for Animal Research (CEUA IPEN 120/13). The bone sample assessment was performed using a total of five bovine femurs, one from each animal, which amounted to two fragments of each femur per group.

From the selected bovine femurs, the soft tissues associated with the bone were manually removed with a scalpel and thereby the diaphysis region was extracted. After this cleaning step, samples were designed into an area of 10 mm^2 using a water refrigerated low speed 0.3 mm diamond saw blade (Accutom-5, Struers s/a, Ballerup, Denmark). Additionally, the bone samples were ground until they reached a thickness of 2 mm[20]. After packing the femur diaphysis in Eppendorf tubes with cotton (moist with distilled water), up to 110 samples were randomly distributed between the groups (n = 10) and placed in a freezer at −20 °C for further independent irradiation experiment.

2.2. Irradiation procedure

Ionizing radiation was applied to bone samples (dose rate of 0.79 kGy/h) using a multipurpose irradiator equipped with a Cobalt-60 source (Gammacell, model 220, series 142, manufactured by Atomic Energy of Canada Limited). The gamma irradiation was designed into low-doses (0.002, 0.004 and 0.007 kGy) and high-doses (1, 10, 15, 25, 35, 50 and 60 kGy), all samples received independent doses. Fig. 1 illustrates the processing of bone.

2.3. FTIR spectroscopy

Spectral data were acquired using an FTIR system (Thermo Nicolet 6700, Waltham, MA) which was equipped with an attenuated total reflectance accessory (Smart Orbit, Thermo Scientific, Waltham, MA). This FTIR spectroscopy study was conducted in the MID-infrared region (4000–400 cm^{-1}) with spectral resolution of 4 cm^{-1} and 100 scans. Bone samples were mounted into a diamond crystal with an area of 2.25 mm^2. The most relevant bands present in the spectrum are shown in Table 1.

Prior to analyzing the raw spectra datasets, the 400–1800 cm^{-1} and 2800–3100 cm^{-1} regions were truncated and the quality control procedure resulted in 82 spectra per group. As a preliminary step, we applied a Savitzky-Golay smoothing filter (a second order polynomial with 11 points) followed by baseline correction (iterative polynomial fitting algorithm). Afterwards, spectral data were normalized by a robust normal variate for further absorbance ratios calculation [25–27] . The absorbance ratios and areas under the examined bands are summarized in Table 2.

2.4. Chemometrics

Partial least squares discriminant analysis (PLS-DA) is a method for multivariate data discrimination. A wide variety of applications have been developed in chemometrics, as well as in areas such as genomics, proteomics, metabolomics, and particularly for vibrational spectroscopy [19,32].

Prior to the development of the PLS-DA model, Student's two-sample *t*-test analyses were performed to maximize the differences between doses of ionizing radiation with the control group (supplementary material)[33]. As a result of this process, the following parameters were determined as the most discriminative spectral markers: Carbonate Accumulation, Carbonate to Mineral, Mineral to Matrix, Mineral Maturity, Crystallinity, Secondary Structure of Protein, Area 3070 cm^{-1}, Area 1201 cm^{-1}, Area 1240 cm^{-1}, Area 1317 cm^{-1}, Area 1547 cm^{-1}.

Furthermore, the variable importance in projection (VIP) score was employed in our spectral markers. Basically, VIP summarizes the effect of a feature based on the calculation of a weighted sum of the squared correlations between the PLS-DA components and the original variable. The weights correspond to the percentage variation explained by the PLS-DA component, which indicates how well a group of variables can be considered more important to describe a given model. For a straightforward interpretation of the PLS-DA results, VIP calculation is based on estimating the importance of each spectral marker in the projection used in our PLS-DA model. The advantage of the use of VIP scores is that spectral markers with a high contribution to the model are easily identified for further evaluation. To obtain consistent and representative results, the spectral markers were split into a training set (70 spectra) and a test set (12 spectra) using leave one out cross validation. The Leave One-Out cross validation estimates are obtained by averaging N iterations, where N is the size of the given sample. For each interaction, one of the cases in the sample is left out as a test set and the workflow is applied to the remaining N-1 cases. This process is repeated for all cases, for N instances. All chemometrics

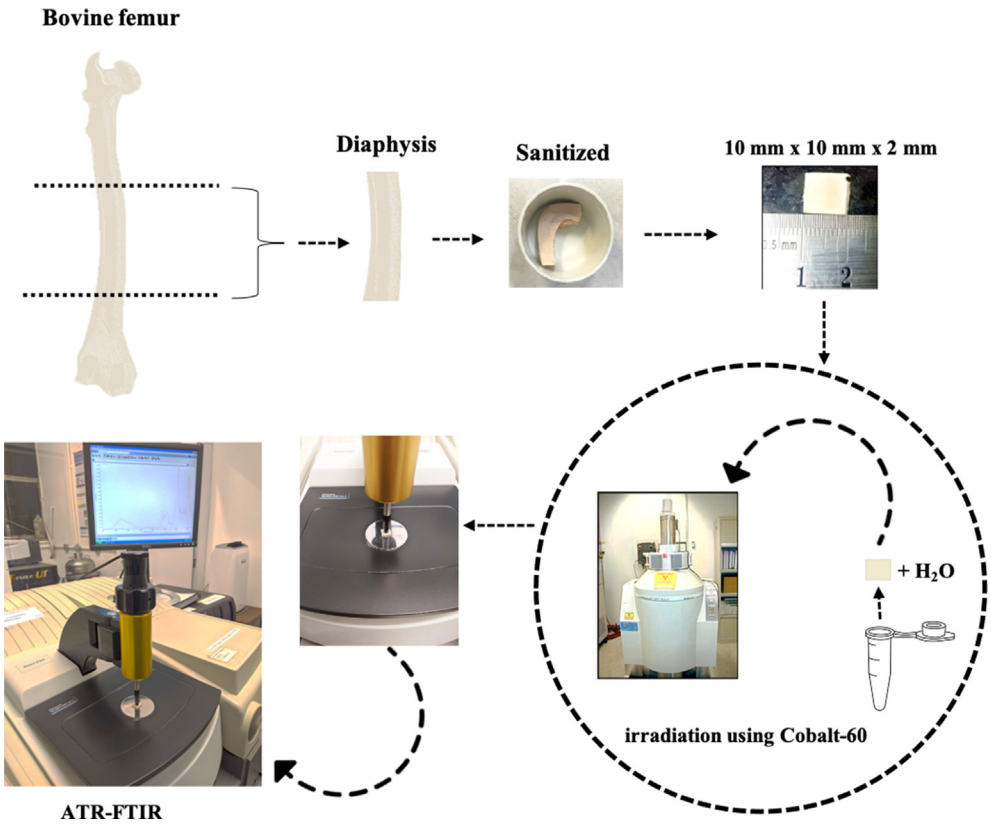

Fig. 1. Schematic bone processing.

Table 1
Bands recorded in bone spectra.

Native (cm^{-1})	Assignment	Ref
563, 604	PO_4^{3-} v_4	[21–23]
870	CO_3^{2-} v_2	[21–23]
956	PO_4^{3-} v_1	[21–23]
1000	PO_4^{3-} v_3	[21–23]
1201	Collagen proteins-amide III	[21–24]
1220	PO_2^- asymmetric	[21–24]
1281	Collagen; Amide III;	[21–24]
1317	Collagen; Amide III;	[21–23]
1340	CH_2 wagging; Collagen;	[21–23]
1406	CH_3 asymmetric deformation	[21–23]
1444	δ(CH_2), lipids, fatty acids	[21–23]
1547	Amide II (δN-H, νC-N)	[21–24]
1635	ß-sheet structure of amide I	[21–24]
1741	ν(C = O)	[21–23]
2854	v_S CH_2	[21–23]
2870	v_S CH_3	[21–23]
2924	v_{AS} CH_2	[21–23]
2958	v_{AS} CH_3	[21–23]
3070	Amide B	[21–23]

assessments were conducted using MATLAB (MathWorks, Natick, MA).

3. Results

Fig. 2 shows average processed FTIR spectra, highlighting the wavenumber regions that represent the most characteristic FTIR bands of bone. All comparisons between ionizing doses with control groups demonstrate a concordance between the band positions, as indicated in our supplementary material (Fig. S1).

The bone is a biological material that contains both inorganic and organic constituents. Firstly, as shown in Fig. 2, the main inorganic components in the bone FTIR spectrum are phosphate (900–1300 cm^{-1}), carbonate (1300–1600 cm^{-1} and 870 cm^{-1}). Secondly, related to the organic matrix, the main components were amide I (1600–1680 cm^{-1}), amide II (1480–1580 cm^{-1}), amide III and collagen (1200–1300 cm^{-1}). Lastly, stretching vibrations related to the CH, CH_2 and CH_3 groups are presented in the range 2800–3000 cm^{-1} [20,21,31]. Based on these considerations, differences in the IR spectra were evaluated by the assessment of spectral features using PLS-DA.

PLS-DA model using FTIR spectra was built considering the prominent relations and area results. To enable overall sample separation, the scores projection has been implemented for the classification and identification of potential spectral markers, as shown in Fig. 3.

Fig. 3A depicts not only that PLS-DA scores are capable of distinguishing between control group and ionizing doses, but also of differentiating high doses from low doses. As shown in Fig. 3B, the intra-group differences at low doses (0.004 – 0.007 kGy) were noted. Once the PLS-DA has demonstrated its capability to discriminate low doses, a significant difference was found between the 0.007 kGy dose and the other low doses. In fact, the 0.007 kGy are more closely associated with high doses than with low doses.

A depiction of the high doses is given in Fig. 3C. There are three distinct clusters of these ionizing doses. The first region relies on doses of 1 kGy and 10 kGy, showing noticeable differences in terms of classification. Whilst the overall classification for a bone dose response demonstrated high performance metrics, such as the discrimination of low doses from high doses and ionizing doses from the control group, it may be found that the score projection decreases the detection rate between 15 kGy and 25 kGy. Furthermore, the radiation doses targeting the doses of 15 kGy and 25 kGy show strong links among the first and third clustering, which may suggest a transitional phase in dosimetric responses. Meanwhile, a

Table 2
Biological assignment for bone spectra.

Absorbance ratio	Spectral markers	Ref
604 cm^{-1} / 553 cm^{-1}	Mineral Maturity	[28–30]
1/ FWHM (1000 cm^{-1})	Crystallinity (1/FWHM)	[23,29–31]
1635 cm^{-1} / 1240 cm^{-1}	Secondary Struct. of Proteins	[29,31]
1000 cm^{-1} / 1635 cm^{-1}	Mineral to ECM matrix ratio	[29,31]
870 cm^{-1} / 1635 cm^{-1}	Carbonate Accumulation	[29,31]
(553 + 597) / 1635	Mineral to Matrix ratio	[29,31]
(870) cm^{-1} / (553 cm^{-1} + 597 cm^{-1} + 1000 cm^{-1})	Carbonate to mineral	[29,31]
1635 cm^{-1} / 1000 cm^{-1}	Amide I to phosphate	[29,31]
1547 cm^{-1} / 1000 cm^{-1}	Amide II to phosphate	[29,31]
(1201 cm^{-1} + 1240 cm^{-1} + 1281 cm^{-1}) / 1000 cm^{-1}	Amide III + Collagen to phosphate	[29,31]
(1547 cm^{-1} + 1635 cm^{-1}) / 1000 cm^{-1}	Amide I + Amide II to phosphate	[29,31]
(1201 cm^{-1} + 1240 cm^{-1} + 1281 cm^{-1} + 1635 cm^{-1} + 1547 cm^{-1}) / 1000 cm^{-1}	Amides + Collagen to phosphate	[29,31]

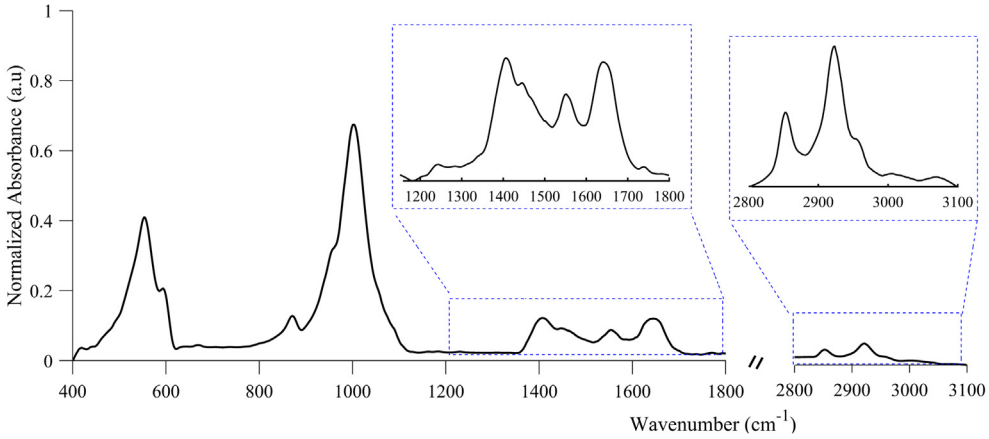

Fig. 2. Representative FTIR spectra of bone.

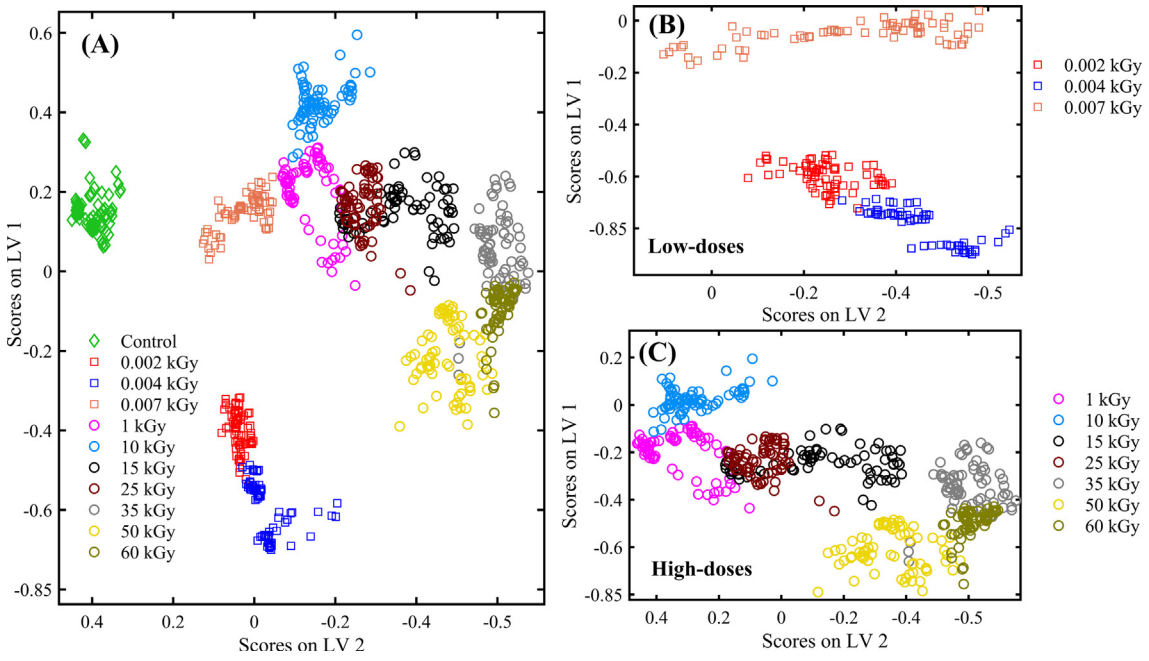

Fig. 3. PLS latent variables (LV) scores from selected spectral features with groups labeled by different colors. (A) LV 1 vs. LV 2 discriminative of all groups. (B) LV 1 vs. LV 2 of low-doses. (C) LV 1 vs. LV 2 of high-doses.

different tendency occurs in the third cluster at doses of 35–60 kGy. There may be other remarkable dose–response patterns that may be contributing to this change in scores projection.

The key objective of using PLS-DA modelling was to identify the significant spectral features and thereby improve the interpretation of bone dose response. As shown in Fig. 4, model performance

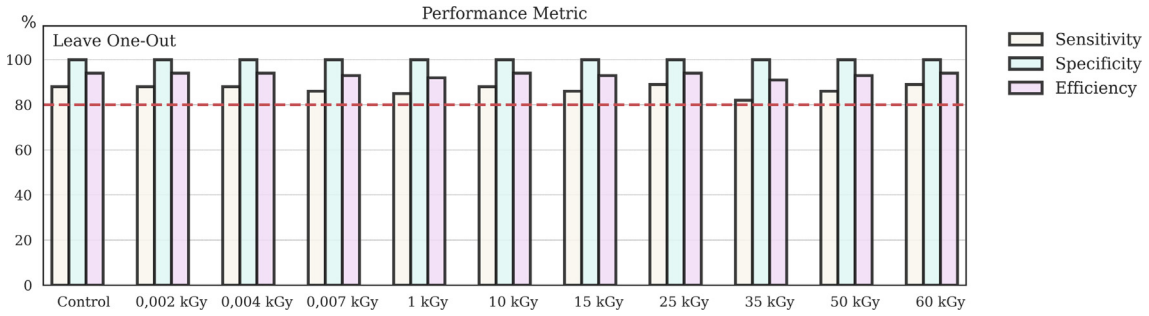

Fig. 4. Performance estimation using Leave One-Out cross validation.

is evaluated according to sensitivity, specificity, and accuracy. For the purposes of assessing its predictive ability, these metrics are supported by the leave-one-out approach.

The Fig. 4 illustrates the stability of the PLS-DA results. As indicated by the red line in Fig. 4, the threshold for beginning the groups comparison is based on metrics higher than 80%. However, while the model may be stable, the critical spectral information remains to be assessed. According to the results of the PLS-DA model, satisfactory changes in bone response could be distinguished by scoring distributions. Despite this, score distributions do not provide sufficient information regarding the predictive significance of spectral features. The variable importance of the projection (VIP) scores, therefore, was applied to rank PLS-DA features, whereby the highest ranked features were likely to provide the most descriptive information for the overall ionizing radiation classification. The evaluation of VIP score is shown in Fig. 5.

The VIP can be used for ranking the spectral features according to their predictive importance in the PLS-DA model. As shown in Fig. 5, with the determination of 1.1 as the threshold value, the spectral features were categorized into two different groups. Those variables for which the VIP scores are less than 1.1 are considered to have a non-significant contribution to the PLS-DA model. The highest contributions (VIP score >1.1) were used to further explain the relationships under the PLS-DA results.

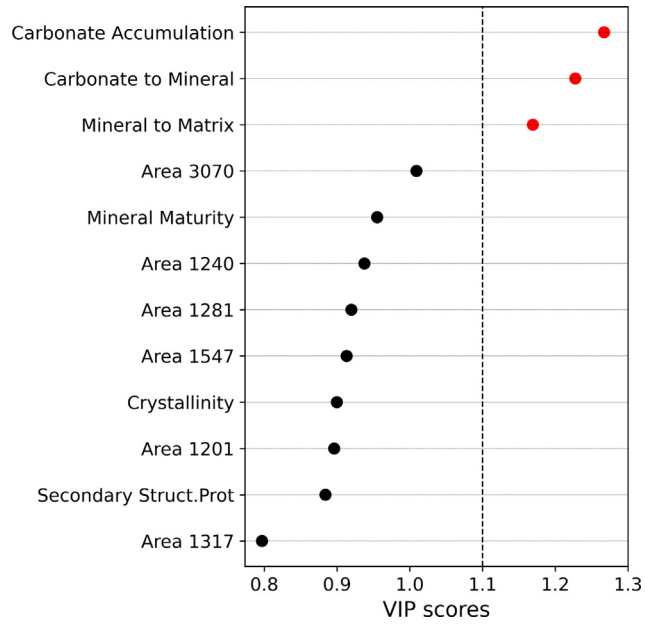

Fig. 5. The VIP score for the PLS-DA analysis. Weighting the predictor variables determines VIP, which is the statistical contribution of the variable to the overall PLS model.

4. Discussion

FTIR spectroscopy identifies subtle changes in the biochemical content of bone material. Because of the inherent complexity of spectra, frequently it becomes challenging to evaluate absorbance variations from the raw data. To overcome this problem, in the present study, pre-processing steps were used for the PLS-DA model to explore the similarities and hidden patterns among ionizing doses. The chemometrics results obtained through VIP scores, indicate carbonate accumulation (CA), carbonate to mineral (CM), and mineral to matrix (MM) as critical spectral features for bone dose response [31].

The effects of bone exposure to ionizing radiation are mediated by two mechanisms: direct and indirect. Firstly, the direct effects are related to the scission sites in the polypeptide chains [23,34]. Secondly, the indirect effects are based on water molecule radiolysis. Free radicals produced by this reaction interact with a wide variety of biomolecules, causing changes in their structure and function [35] . Depending on the dose exposure, this process affects the collagen network of the bone and thereby alters its mechanical properties [36,37].

Irradiated bones are susceptible to side effects [38] which directly alter the activity of cells and repopulation. An aspect of bone recovery in which gluconeogenesis and nucleotide catabolism are downregulated is known as metabolic bone repair. According to Limirio *et al*, this adaptive response was correlated to overexpression in terms of proliferation rate thereby increasing their susceptibility to harmful effects at higher dose levels. Additionally, there is an increase in chemical reactions that lead to the synthesis of amino acids, lipids, proteoglycans, and RNA [38]. In light of this, the motivation behind CA as the strongest VIP score might be because this feature was related with turnover rate, remodeling action, and mineral dissolution, necessary for the reconstruction of new bone tissue [39,40]. According to Kourkomelis *et al*, CA is challenging to evaluate in many FTIR studies due to CA itself does not fully describe each type of possible carbonate content[28,29]. Based on these studies, our findings suggest that CA contributes significantly to changes in the biochemistry of bones after ionizing radiation.

Another essential factor is that ionizing radiation can lead to modifications in the mineral and fiber composition of bone. Both CM (inverse linearly related to elastic modulus) and MM (mineral per amount of collagen present) are presented as important parameters for bone dose response. They determine, in conjunction with CA, the subsequent restoration processes contributing to resorption and formation of bone neoformation [31,41]. Therefore, it is possible that the increasing dose of ionizing radiation contributed to the decrease in bone mineral content [42,43] .

At low dose radiation, the microstructure could be altered significantly [37,44]. Through multimodal validation study, Mandair *et al* report that these low-doses are related to a lower rate of bone

formation. Also, accounting for this tendency to transient differences in collagen crosslink ratios. In fact, these findings exhibited increased bone catabolic and decreased anabolic gene expression [45]. Previous studies investigating the effects of ionizing radiation have shown loss of mechanical properties in grafts associated with Col's fragmentation for 5 kGy [43]. In 2018, Rahman *et al* reported no statistically significant difference in elastic modulus between 18.3 and 21.8 kGy while bone elastic properties significantly decreased following 36.4 kGy [37]. In 2021, Gomes *et al* observed significant structural changes in Col/HAp samples after receiving 17.5 kGy [43]. It also has been reported that changes in the elastic behavior are not observed before 28 kGy, whereas bone strength decreases by 64 % after 28 kGy [46]. Singh *et al* report that the sterilization radiation dose of 25 kGy and 35 kGy did not differ in any significant way, whereas our PLS-DA findings may differ greatly from these results [47]. In fact, doses higher than 30 kGy are required to inactivate HIV in frozen tissues [48,49]. Several studies have shown that ionizing radiation can unfavorably affect the mechanical properties of allografts as well as its chemical composition, but the intrinsic mechanisms responsible for these effects and their consequences *in vivo* are not fully understood [50].

While these studies may have employed other strategies, our results demonstrate that the combination of FTIR spectroscopy with PLS-DA enable the differentiation of the multiple ionizing doses. Through our analysis, we found an association between CA, MM, MA and ionizing dose response. It has been shown that PLS-DA provides accurate boundary classification of the projection scores between 0.002 and 0.007 kGy. Similar trends were observed for 1–10 kGy, 15–25 kGy and 35–60 kGy. Furthermore, the translational utility of our results was enhanced by the consistency in the PLS-DA scores projections with prior studies of bone-ionizing radiation, which have revealed many important dose response patterns.

Assessing the state of bone after ionizing radiation is crucial to highlight radiation dose–dependent changes, which is a critical factor in health management following mass radiation exposure. Toward this direction, a rapid and reliable diagnostic method will be required to reduce the strain on medical resources by identifying the real impact on individuals who have been exposed to radiation [14,15,47,51,52] .

Even though our experimental design was not suitable for the identification of specific molecules when compared to molecular tests, our study indicate that FTIR spectroscopy can detect differences not only between the control group and ionizing radiation dose but can also discriminate between the high and low radiation doses. As a result, FTIR spectroscopy technology could promote the integration of emerging high throughput biodosimetry techniques. These findings can be regarded as a benchmark for future studies, in which additional doses can be incorporated to increase the effectiveness of the model.

5. Conclusion

FTIR spectroscopy technologies provide promising new possibilities in dose response research. In this work, we examine the biochemical effects of ionizing radiation on bone tissues by using the FTIR spectral profile in combination with PLS-DA. Based on these results, FTIR spectroscopy can distinguish the molecular basis for the effects of ionizing radiation and provide comprehensive, objective, and accurate molecular information for diagnosis and treatment evaluation.

In this way, the results presented in this paper contribute to future studies of the dose response to track ionizing radiation effects on biological systems. The results also offer spectral markers, with the support of chemometrics validation, aiming to facilitate the integration of emerging high throughput biodosimetry methods.

CRediT authorship contribution statement

Pedro Arthur Augusto de Castro: Methodology, Software, Data curation, Formal analysis, Writing – original draft. **Derly Augusto Dias:** Investigation, Methodology. **Matheus del-Valle:** Methodology, Software, Validation. **Marcelo Noronha Veloso:** Investigation, Methodology. **Elizabeth Sebastiana Ribeiro Somessari:** Investigation. **Denise Maria Zezell:** Conceptualization, Resources, Funding acquisition, Supervision, Formal analysis, Writing – review & editing.

Declaration of Competing Interest

The authors declare that they have no known competing financial interests or personal relationships that could have appeared to influence the work reported in this paper.

Acknowledgements

This work was supported by FAPESP [17/50332-0 and 21/00633-0], CAPES [Finance Code 001], CAPES/PROCAD [88881.068505/2014-01], and CNPq [INCT-465763/2014-6, Sisfoton 440228/2021-2, PQ-309902/2017-7, PhD-grant-141946/2018-0 and 142229/2019-9].

Appendix A. Supplementary material

Supplementary data to this article can be found online at https://doi.org/10.1016/j.saa.2022.120900.

References

[1] ICRP. https://www.icrp.org/publication.asp?id=ICRP%20Publication%20105 (accessed November 2, 2021).
[2] Global Initiative on Radiation Safety in Health Care Settings. https://www.who.int/initiatives/global-initiative-on-radiation-safety-in-health-care-settings (accessed November 2, 2021).
[3] A. Farooque, R. Mathur, A. Verma, V. Kaul, A.N. Bhatt, J.S. Adhikari, F. Afrin, S. Singh, B.S. Dwarakanath, Low-dose radiation therapy of cancer: role of immune enhancement, Expert Rev. Anticancer Ther. 11 (5) (2011) 791–802, https://doi.org/10.1586/ERA.10.217.
[4] G. Dhawan, R. Kapoor, R. Dhawan, R. Singh, B. Monga, J. Giordano, E.J. Calabrese, Low dose radiation therapy as a potential life saving treatment for COVID-19-induced acute respiratory distress syndrome (ARDS), Radiother. Oncol. 147 (2020) 212–216, https://doi.org/10.1016/J.RADONC.2020.05.002.
[5] J.M. Cuttler, Application of low doses of ionizing radiation in medical therapies, Dose-Response 18 (1) (2020), https://doi.org/10.1177/1559325819895739.
[6] L.E. Feinendegen, Evidence for beneficial low level radiation effects and radiation hormesis, Br. J. radiol. 78 (925) (2005) 3–7, https://doi.org/10.1259/BJR/63353075.
[7] M. Yonezawa, J. Misonoh, Y. Hosokawa, Two types of X-ray-induced radioresistance in mice: presence of 4 dose ranges with distinct biological effects, Mutation Research/Fundamental and Molecular Mechanisms of Mutagenesis 358 (2) (1996) 237–243, https://doi.org/10.1016/S0027-5107(96)00126-1.
[8] L.E. Rutqvist, C. Rose, E. Cavallin-ståhl, A Systematic Overview of Radiation Therapy Effects in Breast Cancer, Acta Oncologica. 42 (5-6) (2003) 532–545, https://doi.org/10.1080/02841860310014444.
[9] G.M. Kendall, C.R. Muirhead, B.H. MacGibbon, J.A. O'Hagan, A.J. Conquest, A.A. Goodill, B.K. Butland, T.P. Fell, D.A. Jackson, M.A. Webb, Mortality and occupational exposure to radiation: first analysis of the National Registry for Radiation Workers., BMJ, Br. Med. J. 304 (6821) (1992) 220–225.
[10] B.P. Fairand, Radiation sterilization for health care products : x-ray, gamma, and electron beam, (2002) 141.
[11] M. Silindir, A.Y. Özer, Sterilization Methods and the Comparison of E-Beam Sterilization with Gamma Radiation Sterilization, J. Pharm. Sci. 34 (2009) 43–53.
[12] R. Singh, D. Singh, A. Singh, Radiation sterilization of tissue allografts: A review, World J. Radiol. 8 (4) (2016) 355, https://doi.org/10.4329/wjr.v8.i4.355.
[13] A. Klein, Y. Bakhshai, F. Roeder, C. Birkenmaier, A. Baur-Melnyk, H.R. Dürr, Technique and results after immediate orthotopic replantation of

extracorporeally irradiated tumor bone autografts with and without fibular augmentation in extremity tumors, BMC Musculoskelet Disord 22 (1) (2021), https://doi.org/10.1186/s12891-021-04629-3.
[14] M.T. Sproull, K.A. Camphausen, G.D. Koblentz, Biodosimetry: A Future Tool for Medical Management of Radiological Emergencies, Health Security. 15 (6) (2017) 599–610.
[15] M. Yadav, S. Bhayana, J. Liu, L. Lu, J. Huang, Y.a. Ma, Z. Qamri, X. Mo, D.S. Jacob, S.T. Parasa, N. Bhuiya, P. Fadda, M. Xu-Welliver, A. Chakravarti, N.K. Jacob, Two-miRNA–based finger-stick assay for estimation of absorbed ionizing radiation dose, Sci. Trans. Medicine. 12 (552) (2020), https://doi.org/10.1126/scitranslmed.aaw5831.
[16] G.A. Carvalho, S. Pilling, Chemical changes induced during heating of acetonitrile-rich ice pre-irradiated by X-rays and its implication in astrochemistry, Spectrochimica Acta Part A: Molecular and Biomolecular Spectroscopy. 267 (2022) 120495, https://doi.org/10.1016/j.saa.2021.120495.
[17] A.C.S. Talari, M.A.G. Martinez, Z. Movasaghi, S. Rehman, I.U. Rehman, Advances in Fourier transform infrared (FTIR) spectroscopy of biological tissues, Appl. Spectroscopy Rev. 52 (5) (2017) 456–506, https://doi.org/10.1080/05704928.2016.1230863.
[18] C. JX, X. XS, Vibrational spectroscopic imaging of living systems: An emerging platform for biology and medicine, Science (New York, N.Y.). 350 (2015). https://doi.org/10.1126/SCIENCE.AAA8870.
[19] C.L.M. Morais, K.M.G. Lima, M. Singh, F.L. Martin, Tutorial: multivariate classification for vibrational spectroscopy in biological samples, Nat Protoc 15 (7) (2020) 2143–2162, https://doi.org/10.1038/s41596-020-0322-8.
[20] D.M. Zezell, C. Benetti, M.N. Veloso, P.A.A. Castro, P.A. Ana, FTIR Spectroscopy Revealing the Effects of Laser and Ionizing Radiation on Biological Hard Tissues, J. Braz. Chem. Soc. 26 (2015) 2571–2582, https://doi.org/10.5935/0103-5053.20150246.
[21] L. Bachmann, R. Diebolder, R. Hibst, D.M. Zezell, Infrared absorption bands of enamel and dentin tissues from human and bovine teeth, Appl. Spectroscopy Rev. 38 (1) (2003) 1–14, https://doi.org/10.1081/ASR-120017479.
[22] Z. Movasaghi, S. Rehman, Dr.I. ur Rehman, Fourier Transform Infrared (FTIR) Spectroscopy of Biological Tissues, Https://Doi.Org/10.1080/05704920701829043. 43 (2008) 134–179. https://doi.org/10.1080/05704920701829043.
[23] N.S. El-Hansi, H.H. Said, O.S. Desouky, M.A. Khalaf, M.S. Talaat, A.M. Sallam, XRD and ATR-FTIR techniques for integrity assessment of gamma radiation sterilized cortical bone pretreated by antioxidants, Cell Tissue Bank 22 (2) (2021) 305–321.
[24] M. Diem, Appendix F: Infrared and Raman Spectra of Selected Cellular Components, Modern Vibrational Spectroscopy and Micro-Spectroscopy. (2015) 399–404, https://doi.org/10.1002/9781118824924.APP6.
[25] E.E. Storey, A.S. Helmy, Optimized preprocessing and machine learning for quantitative Raman spectroscopy in biology, J. Raman Spectrosc. 50 (2019) 958–968, https://doi.org/10.1002/JRS.5608.
[26] M.J. Baker, J. Trevisan, P. Bassan, R. Bhargava, H.J. Butler, K.M. Dorling, P.R. Fielden, S.W. Fogarty, N.J. Fullwood, K.A. Heys, C. Hughes, P. Lasch, P.L. Martin-Hirsch, B. Obinaju, G.D. Sockalingum, J. Sulé-Suso, R.J. Strong, M.J. Walsh, B.R. Wood, P. Gardner, F.L. Martin, Using Fourier transform IR spectroscopy to analyze biological materials, Nat Protoc 9 (8) (2014) 1771–1791.
[27] D.C. Patel, M.F. Wahab, T.C. O'Haver, D.W. Armstrong, Separations at the Speed of Sensors, Anal. Chem. 90 (5) (2018) 3349–3356.
[28] N. Kourkoumelis, M. Tzaphlidou, Spectroscopic assessment of normal cortical bone: Differences in relation to bone site and sex, TheScientificWorldJournal. 10 (2010) 402–412, https://doi.org/10.1100/TSW.2010.43.
[29] N. Kourkoumelis, X. Zhang, Z. Lin, J. Wang, Fourier Transform Infrared Spectroscopy of Bone Tissue: Bone Quality Assessment in Preclinical and Clinical Applications of Osteoporosis and Fragility Fracture, Clinic Rev Bone Miner Metab 17 (1) (2019) 24–39.
[30] G. Dal Sasso, Y. Asscher, I. Angelini, L. Nodari, G. Artioli, A universal curve of apatite crystallinity for the assessment of bone integrity and preservation, Sci Rep 8 (1) (2018), https://doi.org/10.1038/s41598-018-30642-z.
[31] B. Gieroba, A. Przekora, G. Kalisz, P. Kazimierczak, C.L. Song, M. Wojcik, G. Ginalska, S.G. Kazarian, A. Sroka-Bartnicka, Collagen maturity and mineralization in mesenchymal stem cells cultured on the hydroxyapatite-based bone scaffold analyzed by ATR-FTIR spectroscopic imaging, Mater. Sci. Eng., C 119 (2021) 111634, https://doi.org/10.1016/j.msec.2020.111634.
[32] G.L. Erny, E. Brito, A.B. Pereira, A. Bento-Silva, M.C. Vaz Patto, M.R. Bronze, Projection to latent correlative structures, a dimension reduction strategy for spectral-based classification, RSC Adv. 11 (47) (2021) 29124–29129, https://doi.org/10.1039/D1RA03359J.
[33] M. Krzywinski, N. Altman, Comparing samples-part i, Nat. Methods 11 (3) (2014) 215–216.
[34] A. Dziedzic-Goclawska, A. Kaminski, I. Uhrynowska-Tyszkiewicz, W. Stachowicz, Irradiation as a safety procedure in tissue banking, Cell Tissue Banking 6 (3) (2005) 201–219.
[35] G.C. Jagetia, T.K. Reddy, Modulation of radiation-induced alteration in the antioxidant status of mice by naringin, Life Sci. 77 (7) (2005) 780–794.
[36] O. Akkus, R.M. Belaney, P. Das, Free radical scavenging alleviates the biomechanical impairment of gamma radiation sterilized bone tissue, Journal of Orthopaedic Research : Official Publication of the Orthopaedic Research, Society. 23 (4) (2005) 838–845.
[37] N. Rahman, R. Khan, S. Badshah, Effect of x-rays and gamma radiations on the bone mechanical properties: literature review, Cell Tissue Banking 19 (4) (2018) 457–472.
[38] L. PHJO, S. PBF, E. ETP, L. CCA, R. FS, B. JD, R. GD, D. P, Ionizing radiation and bone quality: time-dependent effects, Radiation Oncology (London, England). 14 (2019). https://doi.org/10.1186/S13014-019-1219-Y.
[39] S. Huang, M. Jin, N. Su, L. Chen, New insights on the reparative cells in bone regeneration and repair, Biol. Rev. 96 (2) (2021) 357–375.
[40] M. Bais, J. McLean, P. Sebastiani, M. Young, N. Wigner, T. Smith, D.N. Kotton, T. A. Einhorn, L.C. Gerstenfeld, M.H. Sham, Transcriptional Analysis of Fracture Healing and the Induction of Embryonic Stem Cell-Related Genes, PLoS ONE 4 (5) (2009) e5393, https://doi.org/10.1371/journal.pone.0005393.
[41] S.C. Lucatto, A. Guilherme, L.L. Dib, H.R.C. Segreto, M.T.d.S. Alves, E.H. Gumieiro, R.S. Jahn, R.A. Leite, Effects of ionizing radiation on bone neoformation: histometric study in Wistar rats tibiae, Acta Cirúrgica Brasileira. 26 (6) (2011) 475–480, https://doi.org/10.1590/S0102-86502011000600012.
[42] N. Rahman, R. Khan, T. Hussain, N. Ahmed, Investigation of the mechanism of gamma irradiation effect on bovine bone, Cell Tissue Bank 21 (2) (2020) 249–256.
[43] A.D. Gomes, A.A.R. de Oliveira, M. Houmard, E.H.M. Nunes, Gamma sterilization of collagen/hydroxyapatite composites: Validation and radiation effects, Appl. Radiat. Isot. 174 (2021) 109758, https://doi.org/10.1016/j.apradiso.2021.109758.
[44] E.R. Bandstra, M.J. Pecaut, E.R. Anderson, J.S. Willey, F. De Carlo, S.R. Stock, D.S. Gridley, G.A. Nelson, H.G. Levine, T.A. Bateman, Long-Term Dose Response of Trabecular Bone in Mice to Proton Radiation, Radiation Research. 169 (6) (2008) 607–614, https://doi.org/10.1667/RR1310.1.
[45] G.S. Mandair, M.E. Oest, K.A. Mann, M.D. Morris, T.A. Damron, D.H. Kohn, Radiation-induced changes to bone composition extend beyond periosteal bone, Bone Reports. 12 (2020) 100262, https://doi.org/10.1016/j.bonr.2020.100262.
[46] Biochemical properties of cortical allograft bone using a new method of bone strength measurement. A comparison of fresh, fresh-frozen and irradiated bone - PubMed, (n.d.). https://pubmed.ncbi.nlm.nih.gov/8636167/ (accessed November 2, 2021).
[47] R. Singh, A. Singh, The potential of radiation sterilized and banked tissue allografts for management of nuclear casualties, Cell Tissue Banking 2021 (2021) 1–10, https://doi.org/10.1007/S10561-021-09946-4.
[48] M.A. Moore, Inactivation of enveloped and non-enveloped viruses on seeded human tissues by gamma irradiation, Cell Tissue Bank 13 (3) (2012) 401–407.
[49] D.M. Squillace, Z. Zhao, G.M. Call, J. Gao, J.Q. Yao, Viral Inactivation of Human Osteochondral Grafts with Methylene Blue and Light, Cartilage. 5 (1) (2014) 28–36, https://doi.org/10.1177/1947603513509650.
[50] C.M. Callaghan, M.M. Hasibuzzaman, S.N. Rodman, J.E. Goetz, K.A. Mapuskar, M.S. Petronek, E.J. Steinbach, B.J. Miller, C.F. Pulliam, M.C. Coleman, V.V. Monga, Neoadjuvant radiotherapy-related wound morbidity in soft tissue sarcoma: perspectives for radioprotective agents, Cancers 12 (8) (2020) 2258, https://doi.org/10.3390/CANCERS12082258.
[51] H.E. Schwartz, M.J. Matava, F.S. Proch, C.A. Butler, A. Ratcliffe, M. Levy, D.L. Butler, The Effect of Gamma Irradiation on Anterior Cruciate Ligament Allograft Biomechanical and Biochemical Properties in the Caprine Model at Time Zero and at 6 Months after Surgery, Am. J. Sports Med. 34 (11) (2006) 1747–1755, https://doi.org/10.1177/0363546506288851.
[52] M.M. Pendleton, S.R. Emerzian, S. Sadoughi, A. Li, J.W. Liu, S.Y. Tang, G.D. O'Connell, J.D. Sibonga, J.S. Alwood, T.M. Keaveny, Relations Between Bone Quantity, Microarchitecture, and Collagen Cross-links on Mechanics Following In Vivo Irradiation in Mice, JBMR Plus. 5 (11) (2021), https://doi.org/10.1002/jbm4.v5.1110.1002/jbm4.10545.